Materials Research Express

PAPER

# Temperature dependence of Raman enhancement induced by Au nanorods array



Materials Research Express

PAPER

RECEIVED
13 December 2017

REVISED
3 January 2018

ACCEPTED FOR PUBLICATION
29 March 2018

PUBLISHED
29 June 2018

# Temperature dependence of Raman enhancement induced by Au nanorods array

**Yanru Xu**[1,2], **Yanqing Wang**[3], **Yixin Chen**[1,2], **Yanan Yue**[1,2,4] **and Jin Jiang**[1,2,4]

[1] Key Laboratory of Hydraulic Machinery Transients, MOE, Wuhan University, Wuhan, 430072, People's Republic of China
[2] School of Power and Mechanical Engineering, Wuhan University, Wuhan, Hubei 430072, People's Republic of China
[3] School of Physics and Electronic-Electrical Engineering, Ningxia University, Yinchuan, 750021, People's Republic of China
[4] Authors to whom any correspondence should be addressed.

**E-mail:** yyue@whu.edu.cn **and** jiangjing423@163.com

**Keywords:** temperature, Raman enhancement, Au nanorod

## Abstract

Temperature is an important factor in operation of plasmon-based devices in terms of optical enhancement and system stability. However, systematic study, especially for the experimental validation for the quantitative analysis of quantum efficiency in optical enhancement is still lack of investigation. In this work, the ordered array of Au nanorods is fabricated on silicon and the Raman enhancement of this SERS (Surface Enhanced Raman Scattering) substrate is systematically investigated experimentally for its temperature-dependent characteristics combined with physical explanations through electromagnetic simulations. The SERS substrate shows significant Raman enhancement of silicon signal over the temperature range of 293 to 424 K. It is found that as temperature is increased, Raman intensity of both bare silicon and SERS substrate is decreased with different slope of 0.0020/K and 0.0026/K, respectively. Besides, it is found that a temperature rise of 130 K results in a decrease of 10.2% in Raman enhancement ratio, agreeing well with calculated value (28.6%) of Raman enhancement factor as the maximum predicted range for perfect theoretical structure. The temperature dependence of Raman shift (the slope) does not differ much. However, the photon frequency of inelastic scattered light for both substrates is different at room temperature (0.35 $cm^{-1}$) which is possibly attributed to the existence of residual stress in SERS substrate. The findings in this work are beneficial to understand the Raman enhancement at elevated temperatures, especially for applications in photovoltaic applications.

## 1. Introduction

Surface-enhanced Raman scattering (SERS) effect is an optical enhancement phenomenon induced by nanostructures, such as metallic colloids [1], self-assembled nanoparticles [2], templated nanopatterns [3] and artificially shaped plasmonic structures [4]. The enhancement of optical processes including incident and scattered electromagnetic field is generated by the coherent oscillation of the conduction electrons confined in subwavelength volumes, named as localized surface plasmon resonance (LSPR) [5]. SERS has become a powerful analytical technique, and can be used to provide non-destructive and sensitive identifications for chemical [2], biological [1], and imaging [6] analytes. Besides material [7], size [1, 2, 8–10] and shape [11–13] of nanostructures, the sensing performance of SERS has also been found dependent on temperature [14, 15].

Macomber *et al* firstly observed that the SERS intensity decreased when solution temperature was raised and found that the changes of adatom concentration were responsible for the revisable phenomenon [14]. By investigation of Raman signal of rhodamine 6G (R6G), Yang *et al* found that the SERS intensity gradually raised from 298 K to a maximum at 313 K and decreased from 313 to 373 K and it was related to the contents changes of complexes. Besides temperature effect controlled by chemical enhancement mechanism, Kwon *et al* [16] and Lang *et al* [17] observed the way of temperature affecting from the aspect of optical property influenced by temperature. They found that increased temperature had an inverse effect on the SERS intensity of probe

molecules deposited on silver island films or gold nanoporous films. Temperature also has an inverse effect on the Raman enhancement factor which has been studied through theory analysis [15–17] except by experiment.

Accompanying with enhanced Raman scattering, the damping of plasma oscillations leads to heat generation at nanoscale [18] which could play a positive [19] or negative [20] role in subwavelength optical devices. It has been studied in our previous work that single microparticle can induce a temperature rise of 58.5 K in substrate under near-field heating [21–23]. The optical/thermal coupling due to photothermal effect on Raman enhancement factor affecting the sensitivity and stability is still an open issue. Usually from the aspect of applications of plasmon-based devices, temperature is an important factor affecting optical enhancement and system stability. As such, the temperature dependence of Raman enhancement induced by metallic nanostructures is of great interest and needs to be verified by experiment.

In this work, Raman signal of silicon is used to study the temperature dependence of SERS effect which has single strong signal and wide applications in electronics and photovoltaics. Ordered array of Au nanorods is prepared on silicon (SERS substrate) to provide enhancement for Raman signal. The surface morphologies of SERS substrate are characterized by using of atomic force microscope (AFM) and scanning electric microscope (SEM), respectively. Based on the observed morphologies of SERS substrate, numerical simulations for the electromagnetic field around Au nanorods are conducted with the finite-difference time-domain (FDTD) method to understand the corresponding physical mechanism.

## 2. Sample preparation and Raman characterization

It has been found that the SERS effect is closely dependent on the size, shape and surface morphology of metallic nanoparticles [1, 2] or nanowires [8–10, 13]. Compared with spherical nanoparticles or ultrathin film prepared by colloid or self-assembling method, preparing nanoparticles or nanorods ranging in periodic arrays can allow for better management of the size, shape, and distribution of particles and their optical properties [3, 10, 24] , which is required in our work. The template-based method is applied here to fabricate sample with periodic array of uniform nanorods. Due to the high stability, Au is used here as the plasmonic material.

Figure 1(a) shows the fabrication process of SERS substrate by employing method of physical vapor deposition using ultrathin alumina membranes (UTAMs) as mask. The purchased polymethyl methacrylate (PMMA)/UTAM has self-organized honeycomb-like nanopores. The average pore size is 95 nm, with a interspacing distance of about 30 nm and thickness of 300 nm. Firstly, the PMMA/UTAM is carefully placed on a silicon wafer with PMMA supporter upside. Then care is taken to immerse the sample vertically in acetone baths to remove the PMMA supporter ensuring that only UTAM is left on silicon which is used as mask for following metallic deposition. At the beginning of film deposition, a 2 nm layer of Cr (99.99%) is thermally evaporated onto UTAM/Si as an adhesion layer. Then a 15 nm thick Au (99.99%) film is deposited on UTAM/Si under a vacuum pressure of $2.5 \times 10^{-4}$ Pa at an evaporation rate of 0.05–0.06 nm $s^{-1}$. The thickness of metallic film is monitored and carefully controlled by crystal oscillator of the evaporator. After that, the UTAM on sample is removed by sodium hydroxide solution, leaving the array of Au nanorods on silicon.

The AFM and SEM images of the prepared SERS substrate are presented in figures 1(b) and (c), respectively. The AFM measurement is performed on a MicroNanoD-5A scanning probe microscope operating in contacting mode. Figures 1(b) and (c) shows that the prepared Au nanorods range in periodic hexagonal array. The height of the Au nanorod is about 16 nm and the average diameter is approximately 45 nm, as evidenced from longitudinal section analysis of height (figure 1(d)) and histogram of size distribution (figure 1(e)). The AFM and SEM images provide a confirmation that Au nanorods are uniform in size and arranged periodically, which are essential for SERS measurement [3].

Figure 2(a) shows the schematic of Raman characterization of SERS substrate and bare siliocn (as control) at elevated temperatures. Stokes Raman spectra are recorded using a spectrometer (B&W Tek) with a 532 nm diode laser. The signal integration time for all data acquisitions is 10 s. The probe of spectrometer is fixed on a 3D microstage to regulate the distance between probe and sample surface aiming at an optimal focus level. During the Raman characterizations, samples are heated from 293 to 424 K. To minimize the effect of nanorod size difference on reliability of Raman signal, we firstly conduct the Raman characterization across the whole sample. Then, we locate the region with the strongest Raman signal and lock the position. Each Raman measurement is conducted more than ten times for averaging. Additionally, all the Raman signals are collected across different focal levels of laser irradiation to minimize the error induced by the thermal expansion effect.

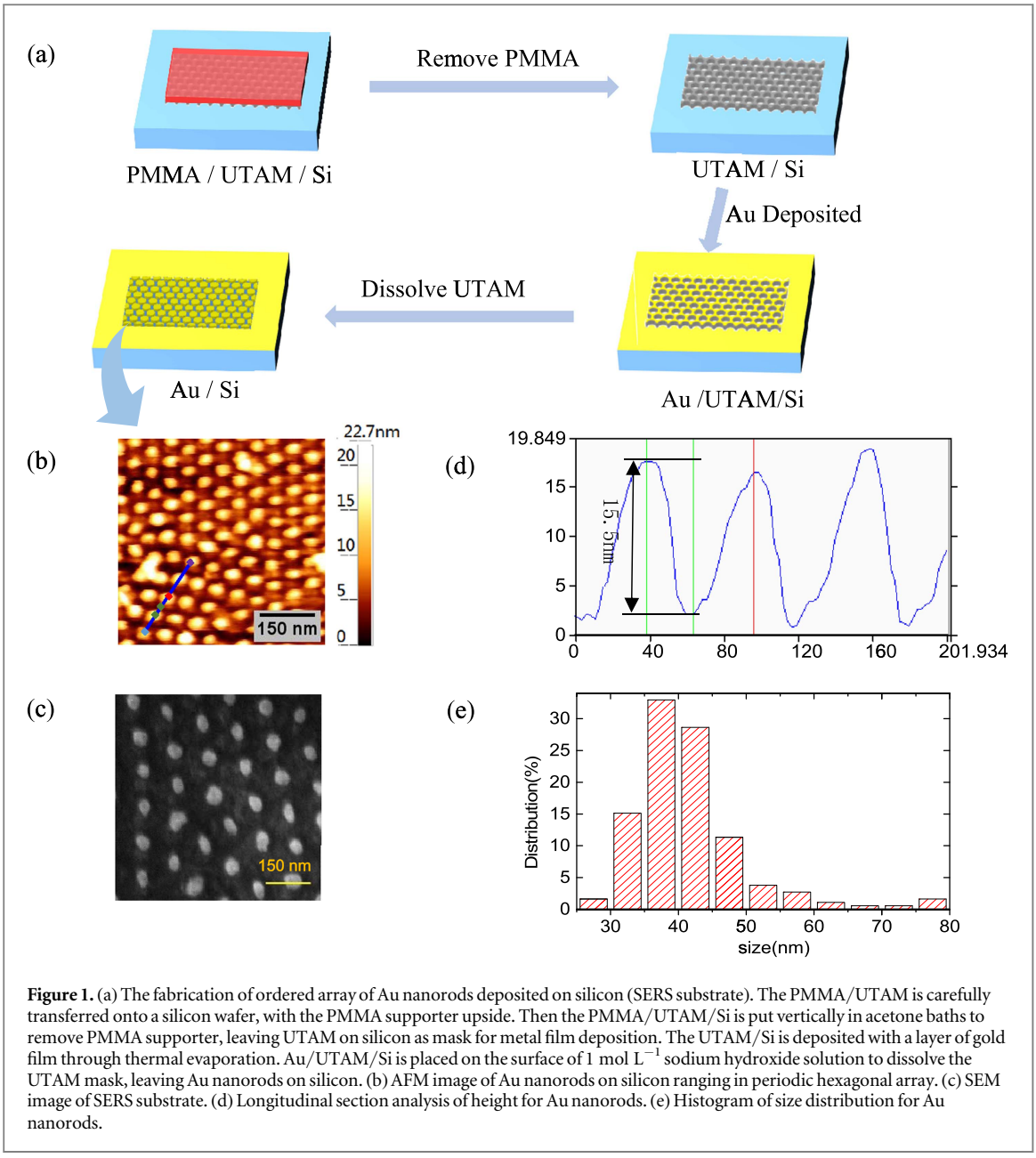


**Figure 1.** (a) The fabrication of ordered array of Au nanorods deposited on silicon (SERS substrate). The PMMA/UTAM is carefully transferred onto a silicon wafer, with the PMMA supporter upside. Then the PMMA/UTAM/Si is put vertically in acetone baths to remove PMMA supporter, leaving UTAM on silicon as mask for metal film deposition. The UTAM/Si is deposited with a layer of gold film through thermal evaporation. Au/UTAM/Si is placed on the surface of 1 mol $L^{-1}$ sodium hydroxide solution to dissolve the UTAM mask, leaving Au nanorods on silicon. (b) AFM image of Au nanorods on silicon ranging in periodic hexagonal array. (c) SEM image of SERS substrate. (d) Longitudinal section analysis of height for Au nanorods. (e) Histogram of size distribution for Au nanorods.

## 3. Results and discussions

### 3.1. Raman enhancement validation and characterization results

Raman spectrum of SERS substrate (red solid line) and bare silicon (black dashed line) measured at room temperture is depicted in figure 2(c). The SERS substrate shows a significant enhancement on silicon signal, the peak intensity at 520 $cm^{-1}$ (Raman shift of single-crystal Si) enhanced by 63% with respect to that of bare silicon. It indicates that the enhancement for Raman signal of silicon is from the ordered array of Au nanorods which has been explained as the excitation of plasmon resonances in nanostructures. This magnitude of enhancement is on the same order as previously reported result. Lorite *et al* [25] investigated an enhancement of about 40% for Raman intensity of silicon covered with Titaniumnitride (TiN) nanostructures compared with that of bare silicon at room temperature. TiN is found to possess similar resonant plasmon properties to gold nanostructures. Due to much thinner film thickness and narrower average gap between Au nanorods, the enhancement ratio here is a little stronger than that of TiN thin film.

The measurement results demonstrate that the Raman intensity, peak shift and Raman enhancement factor from Raman spectra of the SERS substrate is all temperature-dependent. The normalized peak intensity at elevated temperatures of SERS substrate and bare silicon is plotted in figure 3. As temperature is increased, the Raman intensity of bare silicon decreases, which is due to the anharmonicity of vibrational potential energy from optical phonons revealed by previous studies [26, 27]. The intensity of SERS substrate has the same temperature

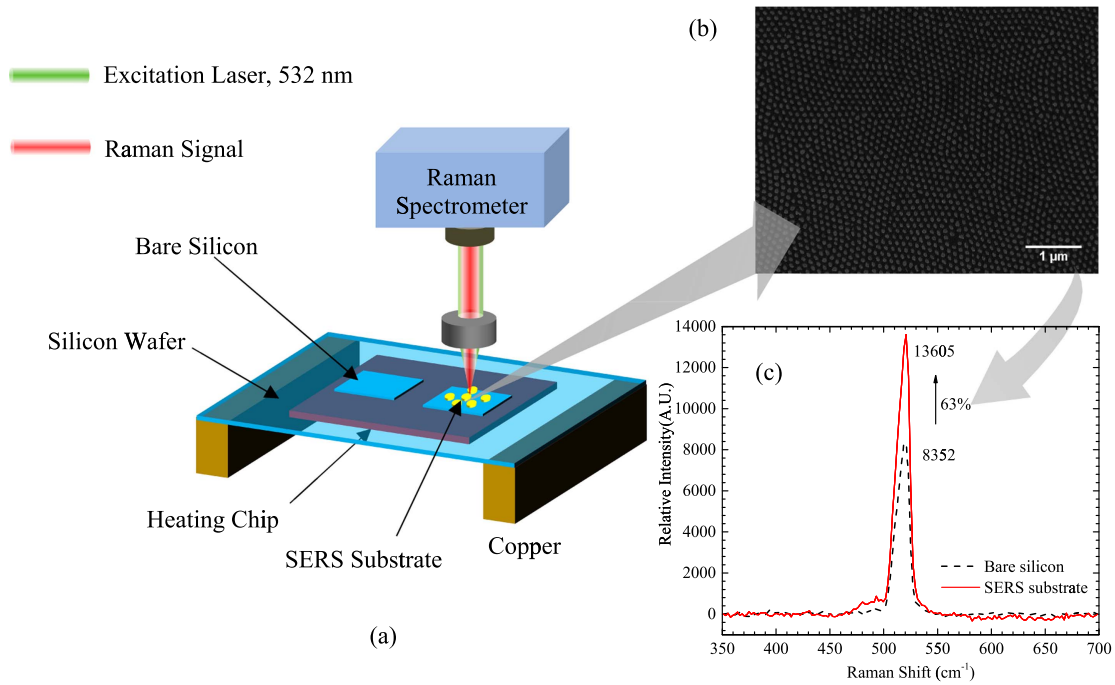


**Figure 2.** (a) Schematic of Raman experiment at elevated temperatures. SERS substrate and bare silicon are glued on a 5 cm × 5 cm silicon wafer heated by a ceramic chip. An optical probe with excitation and collection fibers is fixed on a 3D microstage to collect the Raman signal and transmit it to the Raman spectrometer. (b) The SEM image of SERS substrate with scale bar of 1 $\mu$m showing periodic array of Au nanorods. (c) The Raman spectra of bare silicon (black dashed line) and SERS substrate (red solid line) obtained at room temperature. The SERS substrate shows a significant enhancement on silicon signal, with an enhanced ratio of 63% for the peak intensity with respect to that of bare silicon.

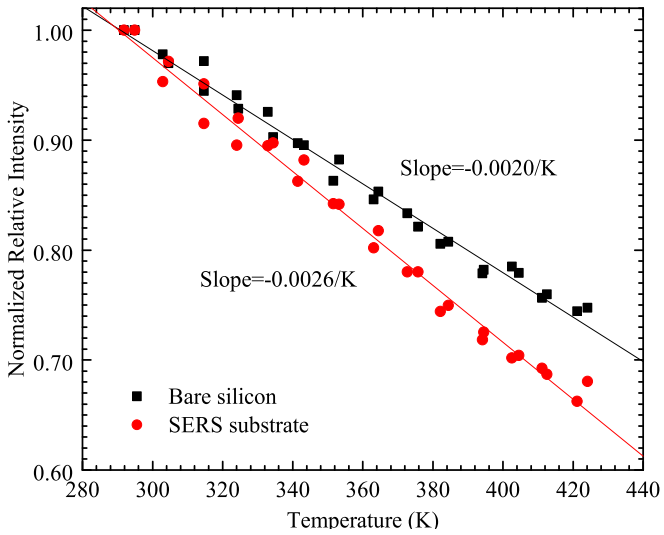


**Figure 3.** Normalized Raman intensity of bare silicon and SERS substrate over the temperature range of 293 to 424 K. As temperature is increased, the peak intensity of bare silicon (black) and SERS substrate (red) both decreases, with slope of −0.0020/K and −0.0026/K, respectively.

dependence. However, their slope is a little different. For SERS substrate, it is $-0.0026\ K^{-1}$, a little higher than that of bare silicon ($-0.0020\ K^{-1}$). Due to the existence of Au nanorods array, the Raman signal from decorated silicon is more sensitive to the variation of temperature.

Raman spectra from two samples are fitted with a Lorentzian function to get peak positions (Raman shift). Figure 4 shows the fitted Raman shift (frequency) versus temperature. When temperature is increased, the phonon frequency of bare silicon exhibits a downshift to lower frequency, which is caused by thermal expansion and anharmonic phonon-phonon coupling [26]. The fitted slope is $-0.022\ cm^{-1}/K$, agreeing well with previous studies [28]. In comparison, the slope for SERS substrate ($-0.023\ cm^{-1}/K$) is not much different. It reveals that

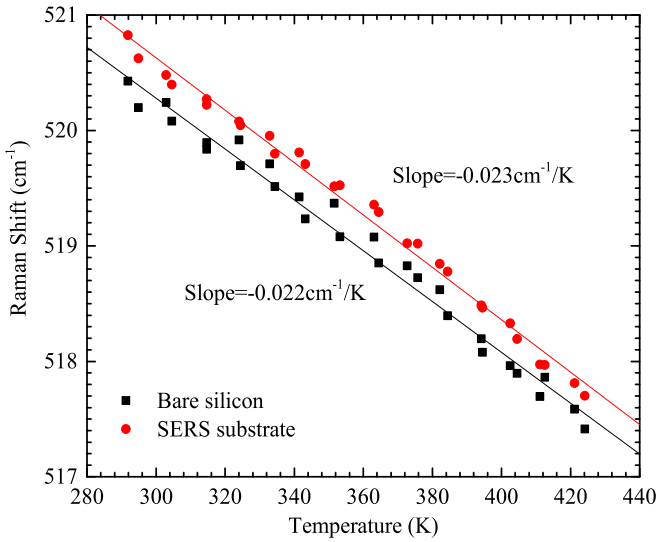


**Figure 4.** The fitted Raman shift of bare silicon (black) and SERS substrate (red) against temperature. The effect of temperature on two samples shows similar. However, their Raman frequency at room temperature is a little different, with a difference value of 0.35 $cm^{-1}$, which may be attributed to the existence of residual stress during sample preparation.

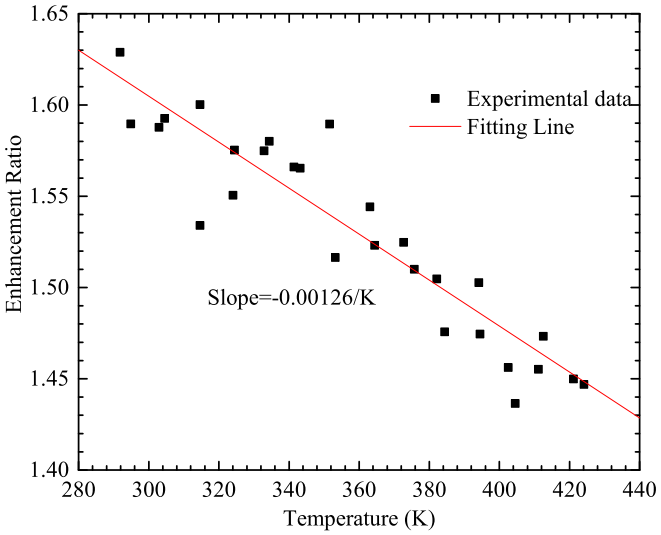


**Figure 5.** The temperature dependence of experimental enhancement ratio, with a slope of $-0.001\ 26\ K^{-1}$. When temperature is increased by 130 K the enhancement ratio is decreased by 10.2%.

the effect of temperature on the Raman frequency of two samples is similar. However, the room-temperature peak frequency is slightly different, with a difference value of 0.35 $cm^{-1}$, as shown in figure 4. It can be understood that the photon frequency of inelastic scattered light for two samples at room temperature is not exactly same. This phenomenon may be attributed to the possible strain effect induced by residual stress formed during the thermal evaporation of gold film [29].

The relationship of Raman enhancement factor with temperature is depicted in figure 5. The enhancement factor at room temperature is 1.6, which is represented as the ratio of SERS peak intensity to normal Raman intensity. As temperature is increased, the enhanced factor exhibits a significant decrease. The fitted slope is $-0.001\ 26\ K^{-1}$, indicating that an increase of 130 K in temperature leads to a decrease of 10.2% in enhancement factor. The measured results demonstrate that the enhanced electromagnetic filed caused by excitation of plasmon resonances in SERS substrate is temperature-dependent and has a inverse relationship with temperature.

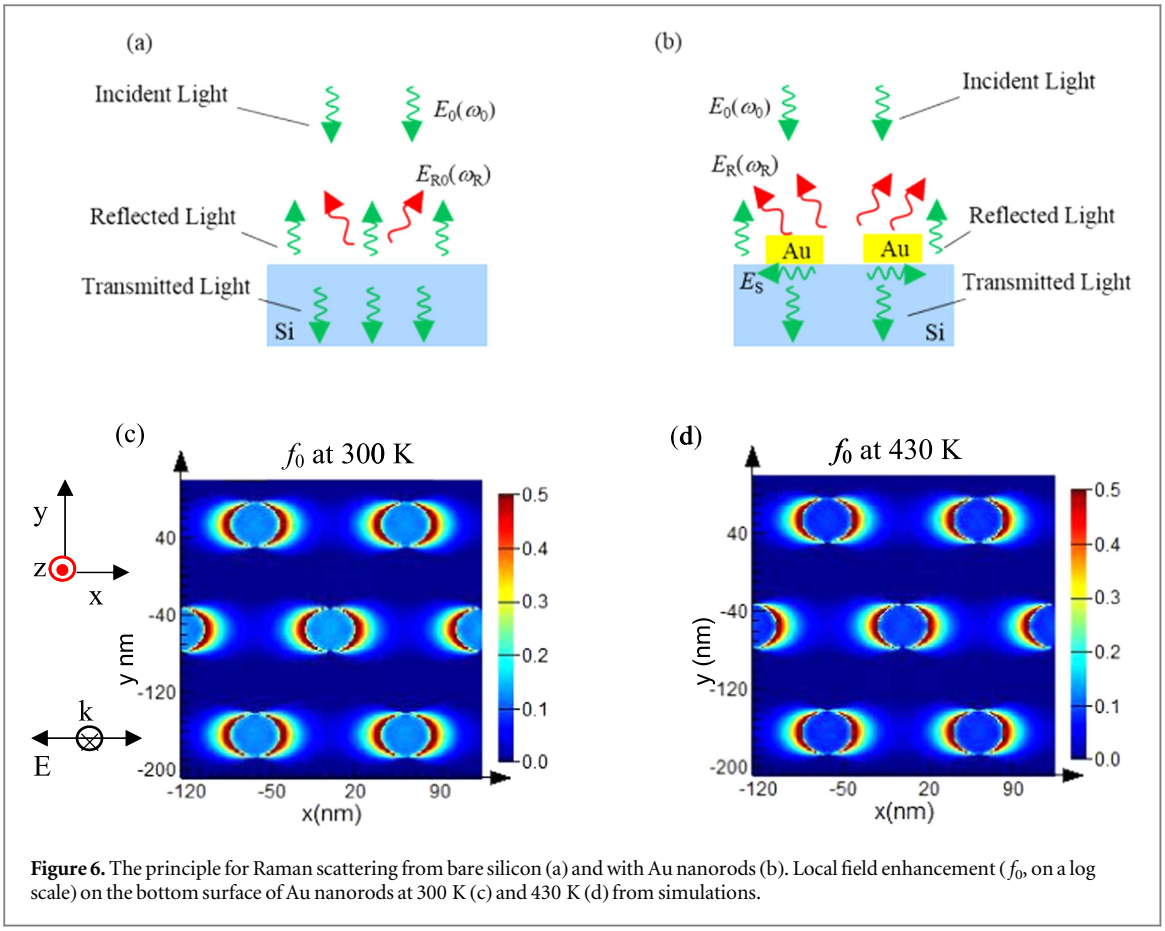


**Figure 6.** The principle for Raman scattering from bare silicon (a) and with Au nanorods (b). Local field enhancement ($f_0$, on a log scale) on the bottom surface of Au nanorods at 300 K (c) and 430 K (d) from simulations.

### 3.2. Numerical simulations for translating experimental observations

The principle for electromagnetic enhancement mechanism for SERS is plotted in figures 6(a), (b). As shown in figure 6(a), when light is irradiated on the silicon, there will be reflection, scattering, transmission and adsorption. For silicon decorated with Au nanorods, its interaction with light become more complex (see figure 6(b)), since the plasmon resonances of Au nanorods are excited which have the ability to enhance the local optical field $\sim E_S(\omega_0)$ at the particle surface compared with the incident field $\sim E_0(\omega_0)$. The local field enhancement factor is denoted as $f_0$ represented as $E_S(\omega_0) \propto f_0 E_0(\omega_0)$. $E_S(\omega_0)$ illuminates the silicon surface and excites inelastic scattering. Under the resonant excitation, the Raman scattered electric field $\sim E_R(\omega_R)$ at frequency $\omega_R$, is also enhanced by a factor of $f_R$. When Raman frequency ($\omega_0 - \omega_R$) is ranged in lower-wavenumber bands, the enhancement factor of Raman scattered field is approximated as $f_R \approx f_0$ [30]. Without consideration of Raman polarizability and Raman tensor, the SERS field enhancement is proportional to the second power of local field enhancement, $E_R(\omega_R) \propto f_0^2 E_0(\omega_0)$. The Raman enhancement factor (the ratio of SERS intensity to normal Raman intensity) is proportional to the fourth power of local field enhancement, $I_R(\omega_R)/I_0(\omega_0) \propto f_0^4$. $f_0^4$ here corresponds to our experimental ratio of SERS peak intensity to Raman intensity without SERS effect.

To understand experimental results, FDTD simulations are performed to study the distribution of electromagnetic field around the Au nanorods and predict the corresponding Raman enhancement ratio with respect to temperature. In our simulations, array of Au nanorods is represented by a hexagonal array of gold cylinders layer for simplification. Simulation region of $750 \times 524 \times 1500$ nm$^3$ ($x \times y \times z$) is used. A 532 nm wave (wavelength used in experiment) is applied as the excitation light source, which irradiates perpendicularly to the sample surface and polarizes along $x$ axis, as shown in figure 6(c). The unit electric field amplitude of 1 V m$^{-1}$ is used for comparison. The distribution of electrical field around the Au nanorods of one period is shown in figure 6(c). The local electric field is evidently enhanced around Au nanorods along the polarization direction. The average and maximum Raman enhancement factor is 14.9 and $6 \times 10^3$ respectively, compared to results in [6]. Note that we use a dielectric function based on results reported in [31] to describe the permittivity of Au nanorods and there is complex interaction of light with silicon in experiment. So the calculated value is higher than the experimental one.

In the calculation of Raman enhancement factors at elevated temperatures, the effect of temperature on the optical property of Au nanorods plays the dominant role. The dielectric function of Au nanorods is expressed as

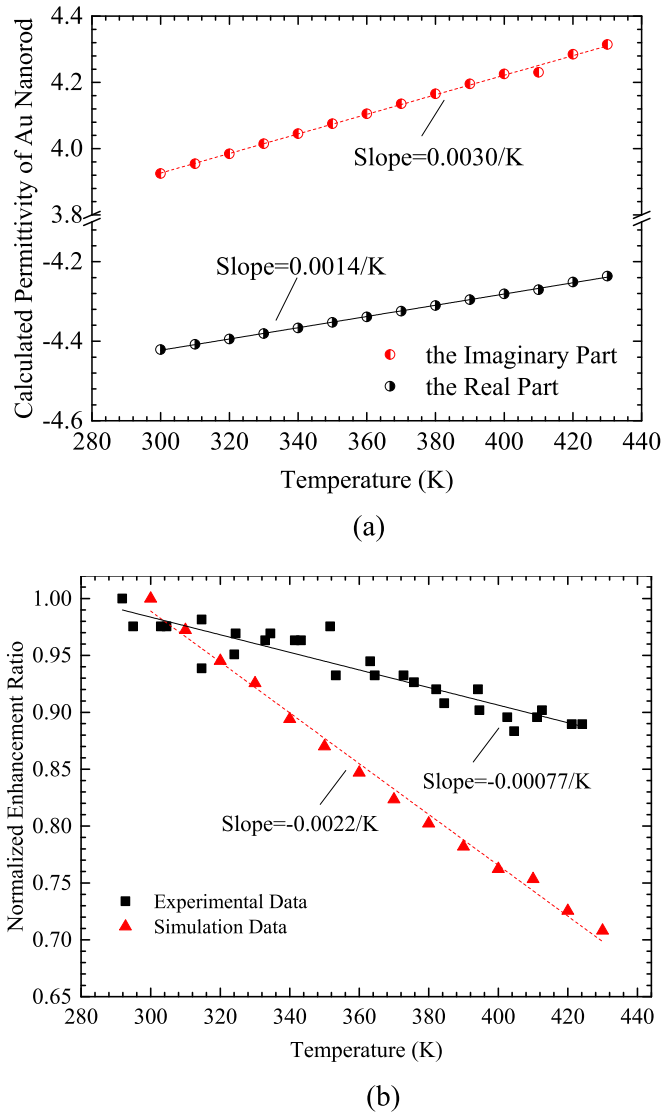


**Figure 7.** (a) The calculated permittivity of Au nanorods under wavelength of 532 nm. (b) Normalized calculated and experimental enhancement factor vs temperature.

$\varepsilon(\omega) = \varepsilon_{\mathrm{ib}}(\omega) + \varepsilon_{\mathrm{D}}(\omega)$ [32], where $\varepsilon_{\mathrm{ib}}$ is the contribution of bound electrons and considered as non-temperature-dependent, and $\varepsilon_{\mathrm{D}}$ is the contribution of the free electrons, which is

$$\varepsilon_{\mathrm{D}}(T, \omega) = 1 - \omega_{\mathrm{p}}^2(T) \cdot [\omega^2 + \mathrm{i}\gamma(\omega, T)\omega]^{-1} \quad (1)$$

where, the plasmon frequency $\omega_{\mathrm{p}}(T)$ [33] and the damping constant of plasma oscillations $\gamma(\omega, T)$ are the terms depending on temperature. $\omega_{\mathrm{p}}(T)$ is derived as $\omega_{\mathrm{P}}(T) = \omega_{\mathrm{p0}} \cdot [1 + \beta(T) \cdot \Delta T]^{-1/2}$ where $\beta(T)$ [33] is the volume expansion coefficient, $\omega_{\mathrm{p0}}$ is the plasmon frequency constant at room temperature, and $\Delta T$ is the temperature difference based on ambient temperature. $\omega_{\mathrm{p}}(T)$ is changed by 0.2% when $T$ is increased by 130 K, showing weak dependence on temperature. The term $\gamma(\omega, T)$ [32] can be expressed by $\gamma(\omega, T) = \gamma_{\mathrm{e-ph}}(T) + \gamma_{\mathrm{s}}(T) + \gamma_{\mathrm{e-e}}(\omega)$, where $\gamma_{\mathrm{e-ph}}(T)$ is the electron-phonon scattering rate, $\gamma_{\mathrm{s}}(T)$ is the surface scattering rate of free electrons and $\gamma_{\mathrm{e-e}}(\omega)$ is the electron-electron scattering rate. $\gamma_{\mathrm{e-ph}}(T)$ [32] is $\gamma_{e-\mathrm{ph}}(T) = S\left[\frac{2}{5} + 4\left(\frac{T}{\theta}\right)^5 \cdot \int_0^{\theta/T} \frac{x^4 \mathrm{d}x}{\mathrm{e}^x - 1}\right]$, where $S$ is a constant, $\theta$ is the Debye temperature for bulk metal, as a constant. When $T$ is increased by 130 K, $\gamma_{\mathrm{e-ph}}$ surges by 1.4 times. $\gamma_{\mathrm{s}}(T)$ [34] is $\gamma_{\mathrm{s}}(T) = A\nu_{\mathrm{F}} \cdot [L_{\mathrm{eff0}} \cdot (1 + \beta \cdot \Delta T)^{1/3}]^{-1}$ which changes by 0.13% with $T$. $\gamma_{\mathrm{e-e}}(\omega)$ [35] has little dependence on temperature, expressed as $r_{e-e}(\omega) = \frac{\omega^2}{4\pi^2\omega_{\mathrm{p0}}}$. Above dielectric function suggests that the electron-phonon scattering rate $\gamma_{\mathrm{e-ph}}(T)$ is the term with strongest dependence on temperature and would play the most important role in the measurement. The calculated dielectric constants of Au nanorods are plotted in figure 7(a). It shows that as temperature is increased by 130 K, the imaginary part of permittivity for Au nanorods increases by 10% and the real part by 4%.

The calculated spatial distribution of filed enhancement at 430 K is shown in figure 6(d). In contrast, the field enhancement at 300 K is a little higher than that at 430 K. The normalized predicted enhancement factor (corresponding to averaged $f_0^4$ on the bottom surface of Au nanorods of one period) as function of temperature is plotted in figure 7(b). The fitting slope is −0.0022/K. When temperature is increased by 130 K, the enhancement factor is decreased by 28.6%, agreeing well with the experimental result (10.2%). Note that we use a dielectric function based on previous results to describe the temperature-dependent permittivity of Au nanorods and there is complex interaction of light with silicon in experiment. So the decreasing ratio of $f_0^4$ is higher than the experimental value, which is as a variation range of prediction.

The simulation models show that there are three terms contributing to the effects of temperature on dielectric constant of Au nanorods, including $\omega_p(T)$, $\gamma_{e-ph}(T)$ and $\gamma_s(T)$. The decreasing ratio of enhancement factor ($f_0^4$) is 26.9% if only considering the temperature dependence of $\gamma_{e-ph}$ in dielectric function of Au nanorods much higher than that only taking account of $\omega_p(T)$, or $\gamma_s(T)$, which means that the electron-phonon scattering rate contributes 92% to the decreasing of enhancement ratio with temperature. While the plasmon frequency $\omega_p(T)$ and the surface scattering rate of free electrons $\gamma_s(T)$ are not the main contributors to the dependence of enhancement on temperature.

## 4. Conclusion

In this work, systematic study on the temperature dependence of SERS signal from ordered array of Au nanorods decorating silicon is conducted experimentally combined with numerical simulation explanations. Significant enhancement (63%) of Raman intensity is observed in our experiment based on the SERS substrate. Heating experiment results reveal that Raman intensity of both bare silicon and decorated silicon is decreased with increase of temperature, having different slope of 0.0020/K and 0.0026/K, respectively. It is found that an increase of 130 K in temperature leads to a decrease of 10.2% in Raman enhancement factor. We also observe that the photon frequency of inelastic scattered light for SERS substrate and bare silicon is different (0.35 $cm^{-1}$) at room temperature, which is attributed to the existence of residual stress during sample preparation. The calculated enhancement ratio from numerical simulation agrees well with experimental data, which reveals that the effect of temperature on SERS signal is attributed to the temperature dependence of dielectric constants in Au nanorods.

## Acknowledgments

The financial support from the National Natural Science Foundation of China (No. 51576145) is gratefully acknowledged. We acknowledge the nanofabrication assistance from Center for Nanoscience and Nanotechnology at Wuhan University.

## ORCID iDs

Yanan Yue https://orcid.org/0000-0002-3489-3949

## Reference

[1] Kneipp K, Kneipp H, Kartha V B, Manoharan R, Deinum G, Itzkan I, Dasari R R and Feld M S 1998 Detection and identification of a single DNA base molecule using surface-enhanced Raman scattering (SERS) *Phys. Rev.* E **57** 6281–4
[2] Rafailović L D, Gammer C, Srajer J, Trišović T, Rahel J and Karnthaler H P 2016 Surface enhanced Raman scattering of dendritic Ag nanostructures grown with anodic aluminium oxide *RSC Adv.* **6** 33348–52
[3] Fu Q, Zhan Z, Dou J, Zheng X, Xu R, Wu M and Lei Y 2015 Highly reproducible and sensitive SERS substrates with Ag inter-nanoparticle gaps of 5 nm fabricated by ultrathin aluminum mask technique *ACS Appl. Mater. Inter.* **7** 13322–8
[4] Li W Q *et al* 2015 Geometrical and morphological optimizations of plasmonic nanoarrays for high-performance SERS detection *Nanoscale* **7** 15487–94
[5] Moskovits M 2013 Persistent misconceptions regarding SERS *Phys. Chem. Chem. Phys.* **15** 5301–11
[6] Kusch P *et al* 2017 Dual-scattering near-field microscope for correlative nanoimaging of SERS and electromagnetic hotspots *Nano Lett.* **17** 2667–73
[7] Sharma B, Frontiera R R, Henry A I, Ringe E and Van Duyne R P 2012 SERS: materials, applications, and the future *Mater. Today* **15** 16–25
[8] DeVetter B M, Bhargava R and Murphy C J 2014 Computational study of the surface-enhanced Raman scattering from silica-coated silver nanowires *Photochem. Photobiol.* **90** 415–8
[9] Toshiaki K, Naoya K, Takashi Y and Hideki M 2015 Surface-enhanced Raman scattering on gold nanowire array formed by mechanical deformation using anodic porous alumina molds *Appl. Phys. Express* **8** 062002
[10] Mirza J, Martens I, Grüßer M, Bizzotto D, Schuster R and Lipkowski J 2016 Gold nanorod arrays: excitation of transverse plasmon modes and surface-enhanced Raman applications *J. Phys. Chem.* C **120** 16246–53

[11] Zhou Y, Zhou X, Park D J, Torabi K, Brown K A, Jones M R, Zhang C, Schatz G C and Mirkin C A 2014 Shape-selective deposition and assembly of anisotropic nanoparticles *Nano Lett.* **14** 2157–61
[12] Lee B S, Lin D Z and Yen T J 2017 A low-cost, highly-stable surface enhanced Raman scattering substrate by Si nanowire arrays decorated with Au nanoparticles and Au backplate *Sci. Rep.* **7** 4604
[13] Lu G *et al* 2017 Plasmon-mediated surface engineering of silver nanowires for surface-enhanced Raman scattering *J. Phys. Chem. Lett.* **8** 2774–9
[14] Macomber S H and Furtak T E 1983 The influence of temperature on surface enhanced Raman scattering in the electrochemical environment: evidence for adatoms *Solid State Commun.* **45** 267–71
[15] Leung P T, Hider M H and Sanchez E J 1996 Surface-enhanced Raman scattering at elevated temperatures *Phys. Rev.* B **53** 12659–62
[16] Kwon C H, Boo D W, Hwang H J and Kim M S 1999 Temperature dependence and annealing effects in surface-enhanced Raman scattering on chemically prepared silver island films *J. Phys. Chem.* B **103** 9610–5
[17] Lang X Y, Guan P F, Zhang L, Fujita T and Chen M W 2009 Characteristic length and temperature dependence of surface enhanced Raman scattering of nanoporous gold *J. Phys. Chem.* C **113** 10956–61
[18] Yeshchenko O A, Kutsevol N V and Naumenko A P 2016 Light-induced heating of gold nanoparticles in colloidal solution: dependence on detuning from surface plasmon resonance *Plasmonics* **11** 345–50
[19] Atwater H A and Polman A 2010 Plasmonics for improved photovoltaic devices *Nat. Mater.* **9** 205–13
[20] Gerasimov V S, Ershov A E, Gavrilyuk A P, Karpov S V, Ågren H and Polyutov S P 2016 Suppression of surface plasmon resonance in Au nanoparticles upon transition to the liquid state *Opt. Express* **24** 26851–6
[21] Tang X, Xu S and Wang X 2013 Thermal probing in single microparticle and microfiber induced near-field laser focusing *Opt. Express* **21** 14303–15
[22] Tang X, Yue Y, Chen X and Wang X 2012 Sub-wavelength temperature probing in near-field laser heating by particles *Opt. Express* **20** 14152–67
[23] Tang X, Xu S and Wang X 2013 Nanoscale probing of thermal, stress, and optical fields under near-field laser heating *PLOS One* **8** e58030
[24] Zheng Y, Wang W, Fu Q, Wu M, Shayan K, Wong K M, Singh S, Schober A, Schaaf P and Lei Y 2014 Surface-enhanced Raman scattering (SERS) substrate based on large-area well-defined gold nanoparticle arrays with high SERS uniformity and stability *ChemPlusChem.* **79** 1622–30
[25] Lorite I, Serrano A, Schwartzberg A, Bueno J and Costa-Krämer J L 2013 Surface enhanced Raman spectroscopy by titanium nitride non-continuous thin films *Thin Solid Films* **531** 144–6
[26] Burke H H and Herman I P 1993 Temperature dependence of Raman scattering in $Ge_{1-x}Si_x$ alloys *Phys. Rev.* B **48** 15016–24
[27] Hart T R, Aggarwal R L and Lax B 1970 Temperature dependence of Raman scattering in silicon *Phys. Rev.* B **1** 638–42
[28] Yue Y, Chen X and Wang X 2011 Noncontact sub-10 nm temperature measurement in near-field laser heating *Acs Nano* **5** 4466–75
[29] De Wolf I, Jian C and van Spengen W M 2001 The investigation of microsystems using Raman spectroscopy *Opt. Laser. Eng.* **36** 213–23
[30] Moskovits M 2005 Surface-enhanced Raman spectroscopy: a brief retrospective *J. Raman Spectrosc.* **36** 485–96
[31] Johnson P B and Christy R W 1972 Optical constants of the noble metals *Phys. Rev.* B **6** 4370–9
[32] Maurya M R and Toutam V 2016 Size-independent parameter for temperature-dependent surface plasmon resonance in metal nanoparticles *J. Phys. Chem.* C **120** 19316–21
[33] Yeshchenko O A, Bondarchuk I S, Gurin V S, Dmitruk I M and Kotko A V 2013 Temperature dependence of the surface plasmon resonance in gold nanoparticles *Surf. Sci.* **608** 275–81
[34] Coronado E A and Schatz G C 2003 Surface plasmon broadening for arbitrary shape nanoparticles: a geometrical probability approach *J. Chem. Phys.* **119** 3926–34
[35] Yeshchenko O A, Bondarchuk I S, Kozachenko V V and Losytskyy M Y 2015 Photoluminescence of rhodamine 6G in plasmonic field of Au nanoparticles: temperature effects *J. Lumin.* **158** 294–300